Monthly Notices
of the
ROYAL ASTRONOMICAL SOCIETY

MNRAS **495,** 238–248 (2020) doi:10.1093/mnras/staa1047

The mean tilt of sunspot bipolar regions: theory, simulations and comparison with observations

N. Kleeorin,[1,2] N. Safiullin,[3]★ K. Kuzanyan,[4,5] I. Rogachevskii,[1,2]★ A. Tlatov[6]★ and S. Porshnev[3,7]

[1]*Department of Mechanical Engineering, Ben-Gurion University of the Negev, POB 653, 8410530 Beer-Sheva, Israel*
[2]*Nordita, KTH Royal Institute of Technology and Stockholm University, Roslagstullsbacken 23, SE-10691 Stockholm, Sweden*
[3]*Institute of Radioelectronics and Information Technology, Ural Federal University, 19 Mira Street, 620002 Ekaterinburg, Russia*
[4]*IZMIRAN, Troitsk, Moscow Region 108840, Russia*
[5]*Key Laboratory of Solar Activity, National Astronomical Observatories, Chinese Academy of Sciences, 100101 Beijing, China*
[6]*Kislovodsk Mountain Astronomical Station of Pulkovo Observatory, 357700 Kislovodsk, Russia*
[7]*N. N. Krasovskii Institute of Mathematics and Mechanics (IMM UB RAS), 620108 Ekaterinburg, Russia*

Accepted 2020 April 15. Received 2020 April 14; in original form 2020 January 6

ABSTRACT

A theory of the mean tilt of sunspot bipolar regions (the angle between a line connecting the leading and following sunspots and the solar equator) is developed. A mechanism of formation of the mean tilt is related to the effect of the Coriolis force on meso-scale motions of super-granular convection and large-scale meridional circulation. The balance between the Coriolis force and the Lorentz force (the magnetic tension) determines an additional contribution caused by the large-scale magnetic field to the mean tilt of the sunspot bipolar regions at low latitudes. The latitudinal dependence of the solar differential rotation affects the mean tilt, which can explain deviations from Joy's law for the sunspot bipolar regions at high latitudes. The theoretical results obtained and the results from numerical simulations based on the non-linear mean-field dynamo theory, which takes into account conservation of the total magnetic helicity and the budget equation for the evolution of the Wolf number density, are in agreement with observational data of the mean tilt of sunspot bipolar regions over individual solar cycles 15–24.

Key words: dynamo – MHD – Sun: activity – sunspots.

1 INTRODUCTION

The origin of the solar magnetic field and the dynamics of solar activity are the subjects of many studies and discussions (Moffatt 1978; Parker 1979; Krause & Rädler 1980; Zeldovich, Ruzmaikin & Sokoloff 1983; Rüdiger & Hollerbach 2004; Ossendrijver 2003; Brandenburg & Subramanian 2005). Solar magnetic fields are observed in the form of sunspots and active regions. One of the characteristics of the solar bipolar region is the mean tilt. The tilt is defined as the angle between a line connecting the leading and following sunspots and the solar equator.

According to Joy's law, the mean tilt of sunspot bipolar regions increases with latitude (Hale et al. 1919; Howard 1991; Sivaraman, Gupta & Howard 1999; Pevtsov et al. 2014; McClintock, Norton & Li 2014; McClintock & Norton 2016). The mean tilt of these regions is caused by the effect of the Coriolis force on large-scale motions in super-granular turbulent convection (Fisher et al. 2000; Pevtsov et al. 2014). The Coriolis force is proportional to $\sin\phi$, where ϕ is the latitude, so that the main dependence of the mean tilt on latitude is expected to be proportional to $\sin\phi$. The mean tilt of sunspot bipolar regions has also been explained by the onset of the kink instability (Leighton 1969; Longcope et al. 1999; Holder et al. 2004). It can also be affected by the large-scale solar magnetic field (Babcock 1961; Norton & Gilman 2005).

In spite of various theoretical, numerical and observational studies related to the mean tilt (D'Silva & Choudhuri 1993; Kosovichev & Stenflo 2008; Dasi-Espuig et al. 2010; McClintock & Norton 2013; Tlatov et al. 2013; Illarionov, Tlatov & Sokoloff 2015; Tlatov 2015; Tlatova, Vasileva & Pevtsov 2015), some observational features related to the mean tilt of sunspot bipolar regions remain unexplained. From observations (Tlatova et al. 2018), it is known that the latitudinal dependence of the mean tilt of sunspot bipolar regions can deviate from $\sin\phi$. There is a non-zero mean tilt of sunspot bipolar regions at the equator, where the Coriolis force vanishes. In particular, there is a systematic non-zero tilt at the equator, with a negative offset for odd cycles and a positive offset for even cycles. Tlatova et al. (2018) also found that the latitudinal dependence of the tilt varies from one solar cycle to another. In order to investigate

★ E-mail: n.t.safiullin@urfu.ru (NS); gary@bgu.ac.il (IR); tlatov@mail.ru (AT)

the latitudinal dependence of the mean tilt of sunspot bipolar regions and its variations in different solar cycles, Tlatova et al. (2018) used data from a series of magnetic field observations of sunspots from Mount Wilson Observatory that is nearly one century long.

In the present study, we develop a theory of the mean tilt of sunspot bipolar regions, taking into account the effects of the solar large-scale magnetic field and the solar differential rotation on the mean tilt. We perform mean-field simulations using the non-linear mean-field dynamo model, which takes into account conservation of the total magnetic helicity and the budget equation for the evolution of the Wolf number density. We demonstrate that the balance between the Coriolis force and the magnetic tension determines an additional contribution of the large-scale magnetic field to the mean tilt of sunspot bipolar regions at low latitudes. We also show that the latitudinal dependence of the solar differential rotation affects the mean tilt, explaining the observed deviations from Joy's law for the mean tilt for sunspot bipolar regions at higher latitudes. Our theoretical and numerical results are compared with the latitudinal dependence of the mean tilt found in observations during the last nine solar cycles.

2 THEORY FOR THE MEAN TILT OF SUNSPOT BIPOLAR REGIONS

The mean tilt of sunspot bipolar regions is determined mainly by the effect of the Coriolis force on meso-scale motions of super-granular convection and large-scale meridional circulation. We use the momentum, induction and entropy equations, applying the anelastic approximation and neglecting dissipation at the boundary between the solar convective zone and the photosphere:

$$\frac{\partial \boldsymbol{U}}{\partial t} = -\nabla\left(\frac{P_{\rm tot}}{\rho_0}\right) - \boldsymbol{g}\,S + \frac{1}{4\pi\rho_0}(\boldsymbol{B}\cdot\nabla)\boldsymbol{B} + \frac{\boldsymbol{\Lambda}_\rho}{8\pi\rho_0}\boldsymbol{B}^2 + \boldsymbol{U}\times(2\boldsymbol{\Omega}+\boldsymbol{W}), \quad (1)$$

$$\frac{\partial \boldsymbol{B}}{\partial t} = (\boldsymbol{B}\cdot\nabla)\boldsymbol{U} - (\boldsymbol{U}\cdot\nabla)\boldsymbol{B} - \boldsymbol{B}\,(\nabla\cdot\boldsymbol{U}), \quad (2)$$

$$\frac{\partial S}{\partial t} = -(\boldsymbol{U}\cdot\nabla)S - \frac{\Omega_{\rm b}^2}{g}\,\boldsymbol{U}\cdot\hat{\boldsymbol{r}}, \quad (3)$$

$$\nabla\cdot\boldsymbol{U} = \boldsymbol{\Lambda}_\rho\cdot\boldsymbol{U}, \quad (4)$$

where $\boldsymbol{U}$ and $\boldsymbol{B}$ are the velocity and magnetic fields, $\boldsymbol{W}=\nabla\times\boldsymbol{U}$ is the vorticity, $P_{\rm tot}=P+\boldsymbol{B}^2/8\pi+\boldsymbol{U}^2/2$ is the total pressure, S and P are the entropy and pressure of the plasma, and $\Omega_{\rm b}^2=-(\boldsymbol{g}\cdot\nabla)S_0$. Here, ρ_0 and S_0 are the plasma density and entropy in the basic reference state, $\boldsymbol{\Lambda}_\rho=-\nabla\ln\rho_0$, $\boldsymbol{g}$ is the acceleration due to gravity, $\hat{\boldsymbol{r}}=\boldsymbol{r}/|\boldsymbol{r}|$ is the unit vector in the radial direction, and $\boldsymbol{\Omega}$ is the angular velocity.

2.1 Effect of the large-scale magnetic field on the mean tilt

We decompose the solution of equations (1)–(4) into the sum of the equilibrium fields (denoted with the superscript 'eq'), related to both the meridional circulation and the differential rotation, and perturbations (with a tilde), related to both super-granular motions in the convective zone and rotational motions of sunspots in the photosphere, which contribute to the mean tilt of sunspot bipolar regions; that is, $\boldsymbol{U}=\boldsymbol{U}^{\rm eq}+\tilde{\boldsymbol{u}}$, $\boldsymbol{B}=\boldsymbol{B}^{\rm eq}+\tilde{\boldsymbol{b}}$, $S=S^{\rm eq}+\tilde{s}$ and $P=P^{\rm eq}+\tilde{p}$, where $\tilde{\boldsymbol{u}}=\partial\boldsymbol{\xi}/\partial t+\boldsymbol{v}^{(\rm c)}$ and $\boldsymbol{v}^{(\rm c)}$ is the convective velocity related to the super-granular motions. The equilibrium magnetic field $\boldsymbol{B}^{\rm eq}$ includes the mean magnetic field caused by the dynamo and the magnetic field of bipolar active regions. The magnetic field of the sunspots is much stronger than the mean magnetic field caused by the solar dynamo. Equations (1)–(4) allow us to obtain an equation for small perturbations $\boldsymbol{\xi}$ related to the rotational motions of sunspots at the boundary between the solar convective zone and the photosphere as

$$\frac{\partial^2\boldsymbol{\xi}}{\partial t^2} = -\nabla\left(\frac{\tilde{p}_{\rm tot}}{\rho_0}\right) - \hat{\boldsymbol{r}}(\boldsymbol{\xi}\cdot\hat{\boldsymbol{r}})\left(\Omega_b^{'2}+\Lambda_\rho^2\,U_{\rm A}^2\right) + 2\left(\boldsymbol{U}^{\rm eq}+\boldsymbol{v}^{(\rm c)}\right)\times\boldsymbol{\Omega} + (\boldsymbol{U}_{\rm A}\cdot\nabla)^2\,\boldsymbol{\xi} + \Lambda_\rho\,(\boldsymbol{U}_{\rm A}\cdot\nabla)\left[\hat{\boldsymbol{r}}\,(\boldsymbol{U}_{\rm A}\cdot\boldsymbol{\xi}) - \boldsymbol{U}_{\rm A}(\boldsymbol{\xi}\cdot\hat{\boldsymbol{r}})\right], \quad (5)$$

where $\tilde{p}_{\rm tot}$ are the perturbations of the total pressure, $\Omega_b^{'2}=\Omega_b^2+g(\hat{\boldsymbol{\xi}}\cdot\nabla)S^{\rm eq}/(\hat{\boldsymbol{\xi}}\cdot\hat{\boldsymbol{r}})$, the Alfvén speed is $U_{\rm A}=B^{\rm eq}/(4\pi\rho_0)^{1/2}$, and $\hat{\boldsymbol{\xi}}=\boldsymbol{\xi}/|\boldsymbol{\xi}|$ is the unit vector. To derive equation (5), we rewrite equations (2) and (3) for small perturbations $\tilde{\boldsymbol{b}}$ and $\tilde{s}$ (see equations A1 and A2 in Appendix A), and substitute them into equation (1) rewritten for small perturbations $\boldsymbol{\xi}$. We also assume that

$$|\partial\boldsymbol{\xi}/\partial t| \ll |\boldsymbol{v}^{(\rm c)}|, \quad |\partial\boldsymbol{\xi}/\partial t| \ll |\boldsymbol{U}^{\rm eq}|,$$
$$\Omega \ll \tau_{\rm A}^{-1}, \quad \Omega \ll \tau_c^{-1},$$
$$\tilde{L}_B \gg H_\rho, \quad \tilde{L}_B \gg L_\xi, \quad (6)$$

where $\tau_{\rm A}=L_B/U_{\rm A}$ is the maximum Alfvén time, L_B is the length of the magnetic field line, $\tau_c=H_\rho/v_r^{(\rm c)}$ is the characteristic time associated with convective super-granular motions, $\tilde{L}_B$ is the characteristic spatial scale of the magnetic field $B^{\rm eq}$ variations, L_ξ is the characteristic scale of variations of $\boldsymbol{\xi}$, and $H_\rho=|\nabla\ln\rho_0|^{-1}$ is the density stratification height. We also consider an equilibrium in the absence of rotation.

Let us discuss the physical meaning of the various terms in equation (5). The term $\hat{\boldsymbol{r}}(\boldsymbol{\xi}\cdot\hat{\boldsymbol{r}})\Omega_b^{'2}$ describes the internal gravity waves, while the term $\hat{\boldsymbol{r}}(\boldsymbol{\xi}\cdot\hat{\boldsymbol{r}})\Lambda_\rho^2\,U_{\rm A}^2$ contributes to the slow magneto-acoustic waves. The term $(\boldsymbol{U}_{\rm A}\cdot\nabla)^2\,\boldsymbol{\xi}$ describes the Alfvén waves, and the last two terms ($\propto\Lambda_\rho$) in equation (5) are the magnetic tension in the density-stratified medium, which contribute to the fast magneto-acoustic waves. Other terms are the Coriolis force and the gradient of the total pressure.

We define the tilt of the sunspot bipolar regions using the vector $\boldsymbol{\delta}^{\rm tw}=\nabla\times\boldsymbol{\xi}$, which is related to the perturbations of vorticity, $\tilde{\boldsymbol{w}}\equiv(\partial/\partial t)(\nabla\times\boldsymbol{\xi})\equiv\partial\boldsymbol{\delta}^{\rm tw}/\partial t$. The absolute value $|\boldsymbol{\delta}^{\rm tw}|\approx|\tilde{\boldsymbol{w}}|\,\delta t$ of this vector characterizes the twist of the magnetic field lines that connect the sunspots of opposite magnetic polarity in the bipolar region. During the twist time δt, the perturbations of the vorticity $\tilde{\boldsymbol{w}}$ do not vanish. The direction of the vector $\boldsymbol{\delta}^{\rm tw}$ coincides with that of the vorticity $\tilde{\boldsymbol{w}}$, and is perpendicular to the plane of the twist. Therefore, the radial component of the vector $\boldsymbol{\delta}^{\rm tw}$ at the boundary between the convective zone and the photosphere can characterize the tilt of the sunspot bipolar regions. At this boundary, the magnetic field inside the sunspots is preferably directed in the radial direction. The mean tilt $\gamma\equiv\langle\boldsymbol{\delta}^{\rm tw}\cdot\boldsymbol{e}_B\rangle_{\rm time}$ of sunspot bipolar regions at the surface of the Sun is defined by averaging the scalar product $\boldsymbol{\delta}^{\rm tw}\cdot\boldsymbol{e}_B$ over a time that is longer than the maximum Alfvén time $\tau_{\rm A}$, where $\boldsymbol{e}_B=\boldsymbol{B}^{\rm eq}/B^{\rm eq}$ is the unit vector along the large-scale magnetic field $\boldsymbol{B}^{\rm eq}$.

The details of the derivation of the equation for the mean tilt at the solar surface γ are given in Appendix A. Here we give the derived expression for the mean tilt of the sunspot bipolar regions at the surface as

$$\gamma = \frac{\tau_{\rm A}^2}{2\pi}\left\langle\nabla\times\left(\left(\boldsymbol{U}^{\rm eq}+\boldsymbol{v}^{(\rm c)}\right)\times\boldsymbol{\Omega}\right)\right\rangle_{\rm time}\cdot\boldsymbol{e}_B, \quad (7)$$

where the angular brackets $\langle ... \rangle_{\rm time}$ denote averaging over a time that is longer than the maximum Alfvén time $\tau_{\rm A}$. We also assume that the source of the tilt of the sunspot bipolar regions, $I_\gamma = 2[\nabla \times [(\boldsymbol{U}^{\rm eq} + \boldsymbol{v}^{(c)}) \times \boldsymbol{\Omega}]] \cdot \boldsymbol{e}_B$, is localized at the vicinity of the boundary between the solar convective zone and the photosphere. Calculating the source I_γ and averaging it over a time longer than the maximum Alfvén time, we arrive at the expression for the mean tilt of sunspot bipolar regions as

$$\gamma = -\delta_0 \left[\sin\phi - \cos\phi \, \frac{\tau_c}{\rm R_\odot} \, \frac{\partial \overline{U}_r}{\partial \phi} \right], \tag{8}$$

where $\delta_0 = (1 + \tilde{C})\, \tau_{\rm A}^2 \, \Omega/(2\pi\, \tau_c)$, $\rm R_\odot$ is the solar radius, and ϕ is the latitude. Here we also took into account that $\partial v_r^{(c)}/\partial r \approx -\tilde{C}\, v_r^{(c)}/H_\rho$ and $\langle \partial v_r^{(c)}/\partial \phi \rangle = 0$. The radial mean velocity, $\overline{U}_r$ is estimated as

$$\overline{U}_r = \frac{C_u}{\kappa} \left(\frac{\ell_{\rm top}^2}{\rm R_\odot} \right) \left(\frac{\rho_{\rm bot}}{\rho_{\rm top}} \right) \left(\frac{u_{\rm bot}^2}{\nu_T^{\rm top}} \right) \left(\frac{\partial^2}{\partial \phi^2} \, \frac{\overline{\boldsymbol{B}}^2}{\overline{B}_{\rm eqp}^2} \right)_{\rm bot} \tag{9}$$

(see Appendix B), where $\ell_{\rm top}$ is the integral scale of turbulent motions in the upper part of the convective zone, $\rho_{\rm bot}$ and $\rho_{\rm top}$ are the plasma densities in the bottom and upper parts of the convective zone, respectively, $u_{\rm bot}$ is the characteristic turbulent velocity at the bottom of the convective zone and $\nu_T^{\rm top}$ is the characteristic turbulent viscosity in the upper part of the convective zone, and $\overline{B}_{\rm eqp} = u\sqrt{4\pi\rho}$ is the equipartition magnetic field. The parameter $\kappa \approx 0.3$–0.4 characterizes the fraction of the large-scale radial momentum of plasma that is lost as the plasma crosses the boundary between the convective zone and the photosphere. The constant C_u in equation (9) varies from 0.7 to 1 depending on the radial profile of the mean magnetic field. Substituting equation (9) into equation (8), we obtain the expression for the mean tilt of the sunspot bipolar regions as

$$\gamma = -\delta_0 \Big[\sin\phi - \delta_{_M} \cos\phi \Big], \tag{10}$$

where

$$\delta_{\rm M} = C_{\rm M} \left(\frac{\ell_{\rm top}}{R_\odot} \right)^2 \left(\frac{\rho_{\rm bot}}{\rho_{\rm top}} \right) \left(\frac{\eta_T^{\rm bot}}{\eta_T^{\rm top}} \right) \left(\frac{\tau_c}{\tau_{\rm bot}} \right) \times \left(\frac{\partial^3}{\partial \phi^3} \, \frac{\overline{\boldsymbol{B}}^2}{\overline{B}_{\rm eqp}^2} \right)_{\rm bot}, \tag{11}$$

and $\tau_{\rm bot} = \ell_{\rm bot}/u_{\rm bot}$ is the characteristic turbulent time at the bottom of the convective zone, $C_{\rm M} = 3C_{\rm u}/(\kappa\, {\rm Pr_T}) \approx 10$, ${\rm Pr_T} = \nu_{\rm T}/\eta_{\rm T}$ is the turbulent Prandtl number, and $\eta_{\rm T}$ is the turbulent magnetic diffusion coefficient.

The parameter $\delta_{\rm M}$ describes the magnetic contribution to the mean tilt of the sunspot bipolar regions. The mechanism related to the magnetic contribution to the mean tilt is as follows. The Coriolis force results in the twist of sunspots in the photosphere, and the balance between the Coriolis force and the magnetic tension determines the magnetic contribution $\delta_{\rm M}$ to the mean tilt of the sunspot bipolar regions. The magnetic contribution $\delta_{_M}$ to the mean tilt is important in the vicinity of the equator, where the main contribution caused by the Coriolis force $\propto \sin\phi$ vanishes. Note also that because $\delta_{\rm M} \propto [(\partial^3/\partial\phi^3)(\overline{\boldsymbol{B}}^2/\overline{B}_{\rm eqp}^2)]_{\rm bot}$, the combination of the dipole and quadrupole dynamo modes has a non-zero contribution to $\delta_{\rm M}$ in the vicinity of the equator.

To estimate the mean tilt of the sunspot bipolar regions, we use the values of the governing parameters taken from models of the solar convective zone (see e.g. Baker & Temesvary 1966; Spruit 1974; more modern treatments make little difference to these estimates). In particular, at depth $H \sim 2 \times 10^{10}$ cm (i.e. at the bottom of the convective zone), the magnetic Reynolds number ${\rm Rm^{bot}} = u_{\rm bot}\, \ell_{\rm bot}/\eta = 2 \times 10^9$ (where η is the magnetic diffusion coefficient due to the electrical conductivity of plasma), the turbulent velocity $u_{\rm bot} \sim 2 \times 10^3$ cm s^{-1}, the integral scale of turbulence $\ell_{\rm bot} = 8 \times 10^9$ cm, the plasma density $\rho_{\rm bot} = 2 \times 10^{-1}$ g cm^{-3}, and the turbulent diffusion coefficient $\eta_{\rm T}^{\rm bot} = 5.3 \times 10^{12}$ cm^2 s^{-1}. The density stratification scale is estimated here as $H_\rho^{\rm bot} = \rho/|\nabla\rho| = 6.5 \times 10^9$ cm, and the equipartition mean magnetic field $\overline{B}_{\rm eqp}^{\rm bot} = 3000$ G. In the upper part of the convective zone, say at depth $H \sim 2 \times 10^7$ cm, these parameters are ${\rm Rm^{top}} = u_{\rm top}\, \ell_{\rm top}/\eta = 10^5$, $u_{\rm top} = 9.4 \times 10^4$ cm s^{-1}, $\ell_{\rm top} = 2.6 \times 10^7$ cm, $\rho_{\rm top} = 4.5 \times 10^{-7}$ g cm^{-3}, $\eta_{\rm T}^{\rm top} = 0.8 \times 10^{12}$ cm^2 s^{-1}, $H_\rho^{\rm top} = 3.6 \times 10^7$ cm, and the equipartition mean magnetic field is $\overline{B}_{\rm eqp}^{\rm top} = 220$ G.

Using these estimates, we calculate the parameters δ_0 and $\delta_{\rm M}$, which determine the mean tilt of the sunspot bipolar region. Taking the Alfvén speed $U_{\rm A} = 5 \times 10^4$ cm s^{-1}, and the length of the magnetic field line $L_B = 4H_\rho = 4 \times 10^9$ cm, we obtain the Alfvén time $\tau_{\rm A} = L_B/U_{\rm A} = 10^5$ s. Taking the convective velocity $u_{\rm c} = (3$–$5) \times 10^4$ cm s^{-1}, we obtain the convective time as $\tau_{\rm c} = (2$–$3) \times 10^4$ s. This yields $\delta_0 = 0.3$–0.5 (in radians) and $\delta_{\rm M} = 0.05$–0.2. This implies that the magnetic contribution $\delta_{\rm M}$ to the mean tilt γ is essential in the low-latitude region, where $\sin\phi$ is small.

The main uncertainty in the estimate of the parameter $\delta_{\rm M}$ is related to the estimation of the third derivative of the mean magnetic field with respect to latitude (see equation 11). This is the reason why we use the numerical dynamo model for the estimation of this quantity (see Section 3). The additional uncertainty is related to the parameters of turbulence at the bottom of the solar convective zone, where the Coriolis number ${\rm Co} \equiv 2\Omega\tau \gg 1$, where τ is the characteristic turbulent time. This effect is not taken into account in the standard models of the solar convective zone based on mixing-length theory.

2.2 Effect of the latitudinal dependence of the solar rotation on the mean tilt

In this section, we take into account the effect of the latitudinal dependence of the solar differential rotation on the tilt of the sunspot bipolar regions. In particular, the latitudinal dependence of the solar rotation at the surface of the Sun can be approximated by

$$\Omega = \Omega_0 \left(1 - C_2 \sin^2\phi - C_4 \sin^4\phi\right) \tag{12}$$

(see LaBonte & Howard 1982), where $\Omega_0 = 2.83 \times 10^{-6}$ s^{-1}, $C_2 = 0.121$ and $C_4 = 0.173$. Substituting equation (12) into equation (10) with $\delta_0 = (1 + \tilde{C})\, \tau_{\rm A}^2\, \Omega/(2\pi\, \tau_{\rm c})$, we obtain

$$\gamma = -\tilde{\delta}_0 \Big[\sin\phi + \delta_3 \sin 3\phi - \delta_5 \sin 5\phi - \tilde{\delta}_{\rm M} \left(\cos\phi + \tilde{\delta}_3 \cos 3\phi - \tilde{\delta}_5 \cos 5\phi \right) \Big], \tag{13}$$

where $\tilde{\delta}_0 = C_{\rm D}\, \delta_0$, $\tilde{\delta}_{\rm M} = \delta_{\rm M} \tilde{C}_{\rm D}/16C_{\rm D}$, $C_{\rm D} = 1 - (3C_2 + 5C_4)/4 \approx 0.693$, $\tilde{C}_{\rm D} = 1 - 4C_2 - 2C_4 \approx 0.17$, and $\delta_3 = (4C_2 + 5C_4)/16C_{\rm D} \approx 0.122$, $\delta_5 = C_4/16C_{\rm D} \approx 1.56 \times 10^{-2}$, $\tilde{\delta}_3 = (4C_2 + 3C_4)/\tilde{C}_{\rm D} \approx 4.48$, $\tilde{\delta}_5 = C_4/\tilde{C}_{\rm D} \approx 1.02$. For the derivation of equation (13), we take into account that $\Omega/H_\rho \gg |\partial\Omega/\partial r|$ and $\Omega/H_\rho \gg r^{-1}|\partial\Omega/\partial\theta|$, and we also use identities (A9)–(A12) given in Appendix A.

In Fig. 1, we show the mean tilt $-\gamma$ (solid line) versus latitude ϕ given by equation (13) of our theory, where γ and ϕ are measured in degrees, and we use the following values for the parameters: $\tilde{\delta}_0 = 0.35$, $\delta_3 = 0.12$, $\delta_5 = 1.6 \times 10^{-2}$, $\tilde{\delta}_3 = 4.48$, $\tilde{\delta}_5 = 1.02$ and $\tilde{\delta}_{_M} = 0$ (i.e. the magnetic contribution to the mean tilt of

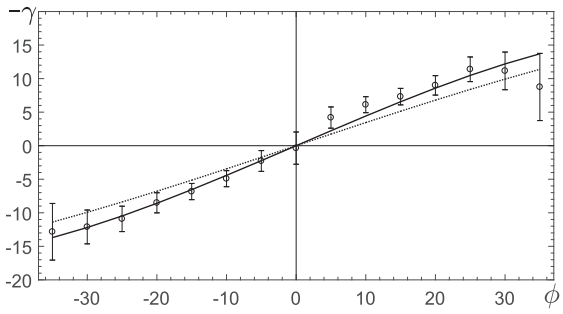

Figure 1. The mean tilt $-\gamma$ (in degrees) versus the latitude ϕ (in degrees): equation (13) of our theory with $\tilde{\delta}_0 = 0.35$, $\delta_3 = 0.12$, $\delta_5 = 1.6 \times 10^{-2}$, $\tilde{\delta}_3 = 4.48$, $\tilde{\delta}_5 = 1.02$ and $\tilde{\delta}_{\rm M} = 0$ (solid line) and the data from observations (circles) of all solar cycles published in fig. 3 of Tlatova et al. (2018). The dotted line corresponds to equation (10) with $\delta_0 = 0.406$ and $\delta_{\rm M} = 0$.

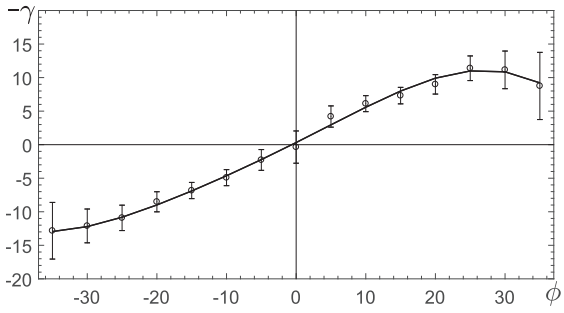

Figure 2. The mean tilt $-\gamma$ (in degrees) versus the latitude ϕ (in degrees): equation (13) of our theory with $\tilde{\delta}_0 = 0.31$, $\delta_3 = 1.26$, $\delta_5 = 0.22$, $\tilde{\delta}_3 = 1.87$, $\tilde{\delta}_5 = 0.78$ and $\tilde{\delta}_{\rm M} = 0.2$ (solid line), and the data from observations (circles) of all solar cycles published in fig. 3 of Tlatova et al. (2018).

the sunspot bipolar regions is neglected here). For comparison with observations, we also show in Fig. 1 the data obtained from observations of all solar cycles presented in fig. 3 of Tlatova et al. (2018), shown here as circles (see Section 4 for more details about the observational data). The observational data have been averaged over bipolar regions of all sizes (see tables 1 and 2 in Tlatova et al. 2018), where the mean value and the standard deviation of Gaussian fittings have been computed. The dotted line in Fig. 1 corresponds to equation (10), which does not take into account the effect of the latitudinal dependence of the solar rotation on the mean tilt. Fig. 1 demonstrates that taking account of the latitudinal part of the differential rotation improves the agreement with observations.

In Fig. 2 we also show the theoretical latitudinal dependence of the mean tilt $-\gamma$ (solid line), taking into account the magnetic contribution to the mean tilt of the sunspot bipolar regions ($\tilde{\delta}_{\rm M} = 0.2$). By slightly varying the values of the other coefficients ($\tilde{\delta}_0 = 0.31$, $\delta_3 = 1.26$, $\delta_5 = 0.22$, $\tilde{\delta}_3 = 1.87$ and $\tilde{\delta}_5 = 0.78$), we obtain a good agreement between the theoretical predictions for the mean tilt and the observational data (see Fig. 2).

3 NUMERICAL MODELLING OF THE MEAN TILT OF SUNSPOT BIPOLAR REGIONS

To obtain the time evolution of the mean tilt of sunspot bipolar regions, and in particular to obtain the butterfly diagram of the mean tilt, we use a non-linear mean-field dynamo model, which is discussed in detail in Kleeorin et al. (2016) and Safiullin et al. (2018). Below, we briefly outline this model. We use spherical coordinates (r, θ, φ) for an axisymmetric large-scale magnetic field, $\overline{\boldsymbol{B}} = \overline{B}_\varphi \boldsymbol{e}_\varphi + \nabla \times (\overline{\mathsf{A}} \boldsymbol{e}_\varphi)$. We consider the mean-field dynamo equations in a thin convective shell, where we take into account the strong variation of the plasma density in the radial direction by averaging the dynamo equations for the mean toroidal field $\overline{B}_\varphi$ and the magnetic potential $\overline{\mathsf{A}}$ of the mean poloidal field over the depth of the convective shell (the so-called no-r dynamo model). We neglect the curvature of the convective shell and replace it by a flat slab (see below). The mean-field dynamo equations for $\overline{B}_\varphi$ and $\overline{\mathsf{A}}$ read

$$\frac{\partial \overline{B}_\varphi}{\partial t} = G D \sin\theta \frac{\partial \overline{\mathsf{A}}}{\partial \theta} + \frac{\partial^2 \overline{B}_\varphi}{\partial \theta^2} - \mu^2 \overline{B}_\varphi, \tag{14}$$

$$\frac{\partial \overline{\mathsf{A}}}{\partial t} = \alpha \overline{B}_\varphi + \frac{\partial^2 \overline{\mathsf{A}}}{\partial \theta^2} - \mu^2 \overline{\mathsf{A}}. \tag{15}$$

In the framework of the no-r model, the last terms on the right-hand side of equations (14) and (15), which determine the turbulent diffusion of the mean magnetic field in the radial direction, are given as $-\mu^2 \overline{B}_\varphi$ and $-\mu^2 \overline{\mathsf{A}}$ (Kleeorin et al. 2016; Safiullin et al. 2018). The differential rotation is characterized by the parameter $G = \partial\Omega/\partial r$, and the parameter μ is determined by the following equation: $\int_{2/3}^{1} (\partial^2 \overline{B}_\varphi / \partial r^2)\, {\rm d}r = -(\mu^2/3)\overline{B}_\varphi$. The dynamo number D in equation (14) is defined as $D = R_\alpha R_\omega$, where $R_\alpha = \alpha_0 {\rm R}_\odot/\eta_{\rm T}$ and $R_\omega = (\delta\Omega)\, {\rm R}_\odot^2/\eta_{\rm T}$. Here the angular velocity $\delta\Omega$ characterizes the differential rotation, and α_0 is the characteristic value of the kinetic part of the α-effect. When the dynamo number is negative, equations (14) and (15) describe the dynamo waves propagating from the central latitudes towards the equator. We use the standard latitudinal profile of the kinetic part of the α-effect as $\alpha(\theta) = \alpha_0 \sin^3\theta \cos\theta$.

Equations (14)–(15) are written in a non-dimensional form, where the length is measured in units of the solar radius ${\rm R}_\odot$, time is measured in units of the turbulent magnetic diffusion time ${\rm R}_\odot^2/\eta_{\rm T}$, the angular velocity $\delta\Omega$ is measured in units of the maximal value of Ω, and α is measured in units of the maximum value of the kinetic part of the α-effect. Here $\eta_{\rm T} = \ell u/3$ is the turbulent magnetic diffusion coefficient, where the integral scale of the turbulent motions ℓ and the turbulent velocity u at the scale ℓ are measured in units of their maximum values through the convective region, and the magnetic Reynolds number ${\rm Rm} = \ell u/\eta$ is defined using the maximal values of the integral scale ℓ and the characteristic turbulent velocity u. The toroidal component of the mean magnetic field $\overline{B}_\varphi$ is measured in units of the equipartition field $\overline{B}_{\rm eqp} = u\sqrt{4\pi\rho_{\rm bot}}$, and the vector potential $\overline{\mathsf{A}}$ of the poloidal component of the mean magnetic field is measured in units of $R_\alpha {\rm R}_\odot \overline{B}_{\rm eqp}$. The density ρ_0 is normalized by its value $\rho_{\rm bot}$ at the bottom of the convective zone. The radius r varies from 2/3 to 1 inside the convective shell, so that the value $\mu = 3$ corresponds to a convective zone with a thickness of about 1/3 of the radius.

Let us discuss the main non-linear effects in the dynamo model. The total α-effect is the sum of the kinetic and magnetic parts, $\alpha = \chi_{\rm v} \Phi_{\rm v}(\overline{B}) + \sigma \chi_{\rm c} \Phi_{\rm m}(\overline{B})$ (Kleeorin et al. 2016; Safiullin et al. 2018), where $\chi_{\rm v} = -(\tau/3)\, \overline{\boldsymbol{u} \cdot (\nabla \times \boldsymbol{u})}$ and $\chi_{\rm c} = (\tau/12\pi\rho)\, \overline{\boldsymbol{b} \cdot (\nabla \times \boldsymbol{b})}$. Here, τ is the correlation time of the turbulent velocity field, $\boldsymbol{u}$ and $\boldsymbol{b}$ are the velocity and magnetic fluctuations, respectively, and $\sigma = \int_{2/3}^{1} (\rho_0(r)/\rho_{\rm bot})^{-1}\, {\rm d}r$.

The magnetic part of the α-effect (Frisch et al. 1975; Pouquet, Frisch & Leorat 1976) and the density of the magnetic helicity are related to the density of the current helicity $\overline{\boldsymbol{b} \cdot (\nabla \times \boldsymbol{b})}$ in the approximation of weakly inhomogeneous turbulent convection (Kleeorin & Rogachevskii 1999). The quenching functions $\Phi_{\rm v}(\overline{B})$ and $\Phi_{\rm m}(\overline{B})$ in the equation for the total α-effect

are given by $\Phi_{\rm v}(\overline{B}) = (1/7)[4\Phi_{\rm m}(\overline{B}) + 3\Phi_{\rm B}(\overline{B})]$ and $\Phi_{\rm m}(\overline{B}) = (3/8\overline{B}^2)\,[1 - \arctan(\sqrt{8}\overline{B})/\sqrt{8}\overline{B}]$ (Rogachevskii & Kleeorin 2000, 2001, 2004), where $\Phi_{\rm B}(\overline{B}) = 1 - 16\overline{B}^2 + 128\overline{B}^4\ln[1 + 1/(8\overline{B}^2)]$, and $\chi_{\rm v}$ and $\chi_{\rm c}$ are measured in units of the maximal value of the α-effect. The function $\Phi_{\rm v}$ describes the algebraic quenching of the kinetic part of the α-effect that is caused by the feedback effects of the mean magnetic field on the turbulent electromotive force. The densities of the helicities and quenching functions are associated with the middle part of the convective zone. The parameter $\sigma > 1$ is a free parameter.

The magnetic part $\alpha_{\rm m}$ of the α-effect is based on two non-linearities: the algebraic non-linearity (quenching of $\alpha_{\rm m}$), given by the function $\Phi_{\rm m}(\overline{B})$, and the dynamic non-linearity. In particular, the function $\chi_{\rm c}(\overline{B})$ is determined by a dynamical equation (Kleeorin & Ruzmaikin 1982; Kleeorin & Rogachevskii 1999; Kleeorin, Rogachevskii & Ruzmaikin 1995; Kleeorin et al. 2000, 2002, 2003a,b; Brandenburg & Subramanian 2005; Zhang et al. 2006, 2012):

$$\frac{\partial\chi_{\rm c}}{\partial t} + \left(\tau_\chi^{-1} + \kappa_{\rm T}\mu^2\right)\chi_{\rm c} = 2\left(\frac{\partial\overline{\rm A}}{\partial\theta}\frac{\partial\overline{B}_\varphi}{\partial\theta} + \mu^2\overline{\rm A}\,\overline{B}_\varphi\right) - \left(\frac{{\rm R}_\odot^2}{2\ell^2}\right)\alpha\,\overline{B}^2 - \frac{\partial}{\partial\theta}\left(\overline{B}_\varphi\frac{\partial\overline{\rm A}}{\partial\theta} - \kappa_{\rm T}\frac{\partial\chi^c}{\partial\theta}\right), \tag{16}$$

where $\boldsymbol{F}_\chi = -\kappa_{\rm T}\nabla\chi_{\rm c}$ is the turbulent diffusion flux of the density of the magnetic helicity, $\kappa_{\rm T}$ is the coefficient of the turbulent diffusion of the magnetic helicity, and $\tau_\chi = \ell^2/\eta$ is the relaxation time of the magnetic helicity. This dynamical equation is derived from the conservation law for the total magnetic helicity. The inverse time τ_χ^{-1} averaged over the depth of the convective zone is given by

$$\tau_\chi^{-1} = H^{-1}\int_{2/3}^{1}\tilde{\tau}_\chi^{-1}(r)\,{\rm d}r \sim \frac{H_\ell\,{\rm R}_\odot^2\,\eta}{H\,\ell^2\,\eta_{\rm T}}, \tag{17}$$

where H is the depth of the convective zone, H_ℓ is the characteristic scale of variations of the integral turbulence scale ℓ, and $\tilde{\tau}_\chi(r) = (\eta_{\rm T}/{\rm R}_\odot^2)(\ell^2/\eta)$ is the non-dimensional relaxation time of the density of the magnetic helicity. The values H_ℓ, η, ℓ in equation (17) are associated with the upper part of the convective zone. The squared mean magnetic field is given by

$$\overline{B}^2 = \frac{2\ell^2}{{\rm R}_\odot^2}\left[\overline{B}_\varphi^2 + R_\alpha^2\left(\mu^2\overline{\rm A}^2 + \left(\frac{\partial\overline{\rm A}}{\partial\theta}\right)^2\right)\right]. \tag{18}$$

Let us discuss the assumptions we use in the mean-field dynamo model that we apply for the numerical mean-field simulations. In the used dynamo model, equations are averaged over the depth of the solar convective zone in the radial direction. Such averaging is undertaken because the fluid density in the solar convective zone is stratified by seven orders of magnitude. There is no numerical dynamo model that is able to take into account such a strong fluid density stratification in the radial direction: the numerical simulations would need to have a very high spatial resolution to resolve a convective zone with such a strong density stratification, and this is not currently possible. That is why we use the no-r dynamo model.

No information is available from the observations about the radial profile of the kinetic helicity and the α-effect in the convective zone of the Sun. This implies that numerical mean-field dynamo models are based on an assumption about the radial profile of the α-effect, which causes uncertainty in the radial profile of the numerical solutions.

On the other hand, three-dimensional mean-field dynamo models allow us to obtain non-axisymmetric dynamo modes and to study non-axisymmetric effects, for example solar active longitudes (Berdyugina et al. 2006; Bigazzi & Ruzmaikin 2004; Pipin & Kosovichev 2015). In particular, observations show that solar activity is distributed non-axisymmetrically, concentrating at 'preferred longitudes'. This effect appears when the solar activity persists within a fixed interval of longitude for a long period of time.

Note also that the radial dependence of the α-effect and differential rotation may give rise to new features. For example, the change in the sign of the α-effect either with radius or with latitude can give a poleward branch of the solar activity (Yoshimura 1981; Glatzmaier 1985; Krivodubskiy 1998). Furthermore, there are indirect signatures that the sign of the observable current helicity, the proxy of the α-effect, changes with depth in the solar convection zone (Kuzanyan et al. 2003). Similarly, in order to obtain simultaneously coexisting poleward and equatorward branches of the dynamo waves, a two-dimensional dynamo model with different signs of the differential rotation can be considered (Belvedere, Kuzanyan & Sokoloff 2000).

The no-curvature assumption is used in the dynamo model to take into account the polar regions, where exact calculations of the Stokes operator require a very high resolution. On the other hand, we use the mean-field numerical simulations only for the calculations of the third-order derivative of the mean magnetic field with respect to the latitude, which is needed to determine the time evolution of the magnetic contribution $\delta_{\rm M}$ to the mean tilt.

The observed solar activity is characterized by the Wolf number (Gibson 1973; Stix 1989), defined as $W = 10g_{\rm w} + f_{\rm w}$, where $g_{\rm w}$ is the number of sunspot groups and $f_{\rm w}$ is the total number of sunspots in the visible part of the Sun. The dynamo model applied in the present study is directly related to the evolution of the Wolf number. In particular, we derive the phenomenological budget equation for the surface density of the Wolf number (Kleeorin et al. 2016; Safiullin et al. 2018), which is given in Appendix C (see equation C1). This equation allows us to perform direct comparisons between the numerical solution of the dynamo equations and the observational data for the evolution of the Wolf number. The budget equation used for the surface density of the Wolf number contains the source term for the sunspot formation (i.e. the rate of production of the Wolf number density) and the sink term describing the decay of sunspots. The rate of increase of the Wolf number density depends on two control parameters: the threshold $\overline{B}_{\rm cr}$ in the mean magnetic field required for the formation of sunspots, and the inverse time $\gamma_{\rm inst}$ of the formation of sunspots. The form of the budget equation for the evolution of the Wolf number is rather general.

As an example for the estimation of the parameters $\overline{B}_{\rm cr}$ and $\gamma_{\rm inst}$, we use the negative effective magnetic pressure instability, which can be excited even for a uniform mean magnetic field. This effect has been investigated in analytical (Kleeorin, Rogachevskii & Ruzmaikin 1989, 1990; Kleeorin, Mond & Rogachevskii 1993, 1996; Kleeorin & Rogachevskii 1994; Rogachevskii & Kleeorin 2007) and numerical (Brandenburg et al. 2011; Brandenburg, Rogachevskii & Kleeorin 2016) studies. This instability results in the formation of magnetic spots (Brandenburg, Kleeorin & Rogachevskii 2013; Brandenburg et al. 2014) and bipolar active regions (Warnecke et al. 2013, 2016).

There is another mechanism for the formation of large-scale inhomogeneous magnetic structures, for example the magnetic buoyancy instability of a stratified continuous magnetic field (Parker 1966, 1979; Gilman 1970; Priest 1982). This instability is excited

when the characteristic scale of the initial mean magnetic field variations is less than the density stratification height-scale. The critical magnetic field $\overline{B}_{\rm cr}$ and the growth rate $\gamma_{\rm inst}$ for the magnetic buoyancy instability can be used for the estimation of the rate of increase of the Wolf number density. For further discussion, see Appendix C.

The observed Wolf number time-series (the monthly mean total sunspot number) have been used for comparison with the results obtained from the mean-field numerical simulations. These observational data are available via open access from the World Data Center SILSO, Royal Observatory of Belgium. The details of the quantitative comparisons between the numerical results and observational data are given in Kleeorin et al. (2016) and Safiullin et al. (2018), and are outlined below.

In the present study, we solve equations (14), (15), (16) and (C1) numerically for the following initial conditions: $\overline{B}_\phi(t=0,\theta) = S_1 \sin\theta + S_2 \sin(2\theta)$ and $\overline{\mathsf{A}}(t=0,\theta)=0$. The parameters of the numerical simulations are as follows: $D=-8450$, $G=1$, $\sigma=3$, $\mu=3$, $\kappa_T=0.1$, $R_\alpha=2$, $\tau_\chi=6.3$, $S_1=0.051$ and $S_2=0.95$. These parameters are chosen in the numerical simulations for the following reasons. In our previous studies (Kleeorin et al. 2016; Safiullin et al. 2018), we performed a parameter scan using about 10^3 runs with different sets of parameters to find an optimal set of parameters to reach a strong correlation between the Wolf numbers obtained in the numerical simulations and observations. There are two crucial parameters that strongly affect the dynamics of the non-linear dynamo system: the dynamo number D and the initial field $B_{\rm init}^{\rm dip}$ for the dipole mode, determined by the parameter S_2. A realistic choice of the initial field $B_{\rm init}^{\rm dip}$ allows very long transient regimes to be avoided.

To find the maximum correlation between the Wolf numbers obtained in the numerical simulations and observations, the following parameter scan was performed: $-8800 \le D \le -8200$ and $0.85 \le S_2 \le 0.95$. The maximum correlation (with about a 70 per cent correlation in observed data and numerical simulations of Wolf numbers) is obtained when the parameters are $D=-8450$ and $S_2=0.95$ (see fig. 12 in Kleeorin et al. 2016). The parameter μ determines the critical dynamo number, $|D_{\rm cr}|$, for the excitation of the large-scale dynamo instability. The flux of the magnetic helicity (see equation 16), characterized by the parameter $\kappa_{\rm T}$, cannot be very small, in order to avoid the catastrophic quenching of the α-effect (Kleeorin et al. 2000, 2002, 2003a,b). The optimal value for this parameter is $\kappa_{\rm T} \approx 0.1$. The variations of the other parameters only weakly affect the obtained results (Kleeorin et al. 2016).

Using the results of these numerical simulations, we plot in Fig. 3 (upper panel) the butterfly diagram of the normalized mean tilt $-\gamma/\tilde{\delta}_0$ given by equation (13), with the magnetic contribution to the mean tilt as

$$\delta_{\rm M}\left(\overline{\boldsymbol{B}}^2\right) = C_*\left(\frac{\partial^3}{\partial\phi^3}\frac{\overline{\boldsymbol{B}}^2}{B_{\rm eqp}^2}\right)_{\rm bot}, \qquad (19)$$

where the parameter $C_*=0.8$. The increase of the values of the mean tilt in the recent three cycles in the low latitudes seen in Fig. 3 (upper panel) can be explained by the joint effect of the dipole and quadrupole dynamo modes. In particular, as follows from the numerical simulations during the non-linear evolution caused by the dynamics of the magnetic helicity in the recent three cycles, the contribution of the dipole dynamo mode to magnetic activity decreases, while the quadrupole dynamo-mode contribution increases. This is in qualitative agreement with observations (Livshits & Obridko 2006). In addition, as follows from observations, during

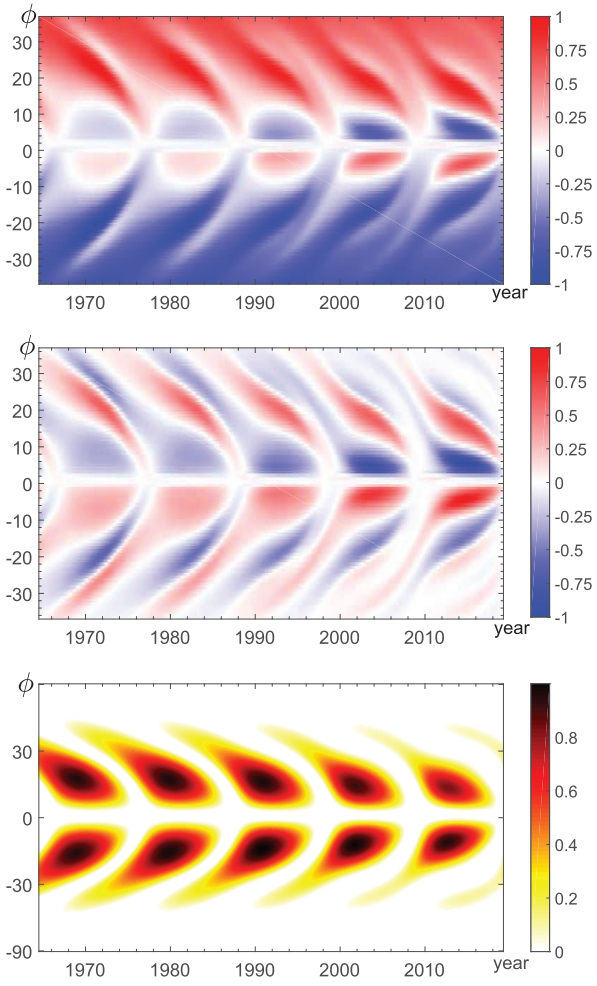

Figure 3. Butterfly diagrams of the normalized mean tilt $-\gamma/\tilde{\delta}_0$ (upper panel) given by equation (13) and the total magnetic contribution $\delta_{\rm M}^*$ to the mean tilt (middle panel) given by the second line of equation (13). Butterfly diagram of the surface density of the Wolf numbers (bottom panel). Here the colour bars are normalized by their maximum values.

the transition from high to low solar cycles, the magnitude of the mean tilt decreases (Dasi-Espuig et al. 2010).

In Fig. 3 (middle panel), we also show the butterfly diagram of the total magnetic contribution $\delta_{\rm M}^* = -\tilde{\delta}_{\rm M}\,(\cos\phi + \tilde{\delta}_3\,\cos 3\phi - \tilde{\delta}_5\,\cos 5\phi)$ to the mean tilt, where the latitudinal part of the differential rotation is taken into account. For comparison, in Fig. 3 (bottom panel), we also plot the butterfly diagram of the surface density of the Wolf numbers. The butterfly diagram of the normalized mean tilt of sunspot bipolar regions is essentially different from that of the surface density of the Wolf numbers. In particular, the mean tilt distribution in both hemispheres is nearly homogeneous; that is, it depends weakly on the phase of the solar cycle except for in small regions at lower latitudes, where the mean tilt has opposite signs in each hemisphere. On the other hand, the distribution of the surface density of the Wolf number is strongly inhomogeneous; that is, it strongly depends on the phase of the solar cycle.

It can be seen from Fig. 3 (middle panel) that around the solar maximum in the middle latitudes (the 'Royal' activity zone), the sign of the magnetic contribution $\delta_{\rm M}^*$ to the mean tilt is the same as that of the contribution caused by the Coriolis force. The 'Royal' activity zone migrates towards lower latitudes for lower solar activity circles

23–24 (see Fig. 3, bottom panel). At lower latitudes (below 10°), the magnetic contribution $\delta^*_{\rm M}$ to the mean tilt is negative/positive in the northern/southern hemisphere (see Fig. 3, middle panel). This effect increases towards lower solar activity circles 23–24. In spite of the fact that the magnetic contribution $\delta^*_{\rm M}$ in lower latitudes is the dominant contribution to the mean tilt of sunspot bipolar regions, its contribution to the mean tilt is also important at latitudes around 25°–30° (see Figs 1–3, upper and middle panels).

4 COMPARISON WITH OBSERVATIONS OF THE MEAN TILT

In this section, we compare our numerical results with observational data of the mean tilt $-\gamma$ of sunspot bipolar regions. We use the observational data that were obtained by Tlatova et al. (2018) from daily sunspot drawings taken at Mount Wilson Observatory (MWO). The data cover a century-long period. The original MWO drawings were digitized using a software package developed by Tlatova et al. (2015, see also references therein). The digitization includes the date and time of observations, the heliographic coordinates of each umbra, its area, and the strength and polarity of its magnetic field. The overall digitized data set used by us contains 20 318 days of observations, from 1917 to 2016 October. The method of Tlatova et al. (2018) enables us to identify clusters of sunspots of positive and negative polarity, from which bipolar pairs formed.

In total, 441 973 measurements of the magnetic field of individual nuclei and pores of sunspots have been carried out, and 51 413 bipolar regions have been allocated. Initially, clusters of active regions of positive and negative polarity were searched for. In order to achieve this, the sunspots were sorted by area for each day of observation, and kernels of the same polarity located at a distance of no more than 10° in longitude and 7° in latitude from the spot of maximum area were selected. For each cluster, the average coordinates were computed using the weight function over the area. Next, a bipole counterpart through clusters of sunspots of negative polarity was found.

There are two types of observational data. The first type of data used in the present study, to produce Figs 1 and 2 (see Section 2), is the result of averaging bipolar pairs of all sizes. This type of data is presented in tables 1 and 2 of Tlatova et al. (2018), where the mean value and the standard deviation of Gaussian fittings were computed. We compared the observational data with the mean tilts obtained from our theoretical and numerical simulations, and found that the theoretical results fit the observations very well. The data were filtered to exclude bipolar regions smaller in length than 3°. In total, there were 18 547 bipolar regions in the even solar cycles and 17 435 in the odd solar cycles. We used bipolar regions larger than 3° because smaller bipolar regions almost do not possess certain tilt angles.

The second type of data, used below to produce Fig. 4, comprises all the data on the tilts of all bipolar regions filtered by the small-sized bipolar pairs, so that only bipolar regions larger than 3° were retained. The cut-off area of those pairs was set to several μH ($4\pi \times 10^{-6}$ of a steradian). We used these data to compare with our theoretical and numerical results based on the time evolution of the mean tilt of sunspot bipolar regions.

Note that both these samplings are very different from what was previously published for the statistics of bipolar regions by Tlatov et al. (2013) and Tlatov (2015). In earlier works, the bipolar regions were composed from individual sunspot nuclei, while in our studies they are formed from clusters of sunspots. Thus, our results may be qualitatively very different from those of Kosovichev & Stenflo (2008) and Dasi-Espuig et al. (2010). Because the nuclei of spots are formed of two opposite polarities, the technique and the results are significantly different.

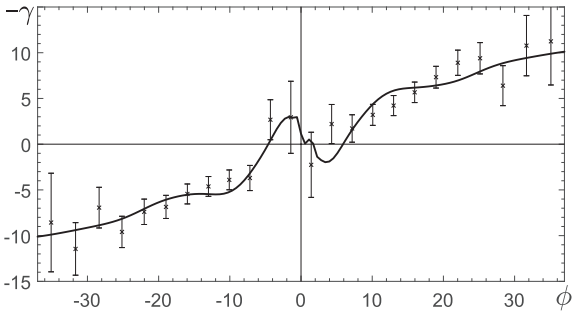

Figure 4. The mean tilt $-\gamma$ (in degrees) versus the latitude ϕ (in degrees): numerical simulations (solid line) and observations of sunspot bipolar regions (crosses) averaged over individual cycles 15–24.

In Fig. 4, we show the mean tilt $-\gamma$ (in degrees) versus the latitude ϕ (solid line) obtained using equation (13), where the magnetic contribution $\delta_{\rm M}$ to the mean tilt is calculated by the mean-field numerical simulation for $C_* = 0.8$, $\delta_0 = 0.29$, $\delta_3 = 0.122$, $\delta_5 = 1.56 \times 10^{-2}$, $\bar{\delta}_3 = 4.48$ and $\bar{\delta}_5 = 1.02$. These numerical results are also compared with the observational data of the mean tilt $-\gamma$ of sunspot bipolar regions. The observational data have been averaged over individual solar cycles (from cycle 15 to cycle 24). The numerical results are also averaged over the same cycles. It follows from Fig. 4 that there is an asymmetry between the northern and southern hemispheres. We stress that we have taken into account here the effect of the latitudinal dependence of the solar differential rotation on the mean tilt of the sunspot bipolar regions, as well as the contribution to the mean tilt caused by the large-scale magnetic field. The theoretical results and the numerical simulations for the mean tilt of sunspot bipolar regions are in agreement with the observational data.

Remarkably, there is a difference between Figs 1 and 4 in the vicinity of the equator. In particular, in Fig. 4 the mean tilt is calculated by averaging over only large-size bipolar regions, and is not zero in the vicinity of the equator. Moreover, the mean tilt of the large-size bipolar regions reverses its sign in the vicinity of the equator, $\phi \approx \pm 5°$. On the other hand, in Fig. 1 the mean tilt is calculated by averaging over active regions of all sizes, and it tends to zero in the vicinity of the equator. An explanation of this phenomenon is given in the next section.

5 THE CONTRIBUTION OF THE CURRENT HELICITY TO THE MEAN TILT

The current helicity, $\langle \boldsymbol{B}^{\rm ar} \cdot \mathbf{curl}\, \boldsymbol{B}^{\rm ar} \rangle$, of the magnetic field, $\boldsymbol{B}^{\rm ar}$, in the active region describes the correlation between the magnetic field and the electric current, and it characterizes the twist of the magnetic field, where the angular brackets denote averaging over the surface occupied by the active region. This implies that the current helicity of the active region should contribute to the total mean tilt. This contribution is given by

$$\gamma_H = L_{\rm ar} \frac{\langle \boldsymbol{B}^{\rm ar} \cdot \mathbf{curl}\, \boldsymbol{B}^{\rm ar} \rangle}{\langle (\boldsymbol{B}^{\rm ar})^2 \rangle}, \qquad (20)$$

where $L_{\rm ar}$ is the characteristic size of an active region. It has been shown by Zhang et al. (2012) that the current helicity of the active region, $\langle \boldsymbol{B}^{\rm ar} \cdot \mathbf{curl}\, \boldsymbol{B}^{\rm ar} \rangle$, is related to the magnetic helicity $\langle \boldsymbol{A}^{\rm ar} \cdot \boldsymbol{B}^{\rm ar} \rangle$

of the active region as

$$\langle \boldsymbol{B}^{\rm ar}\cdot\mathbf{curl}\,\boldsymbol{B}^{\rm ar}\rangle \approx \frac{1}{L_{\rm ar}^2}\,\langle \boldsymbol{A}^{\rm ar}\cdot\boldsymbol{B}^{\rm ar}\rangle + O\left(\frac{L_{\rm ar}^2}{{\rm R}_\odot^2}\right), \tag{21}$$

where $\mathrm{R}_\odot$ is the solar radius. Substituting equation (21) into equation (20), we obtain

$$\gamma_H = \frac{\langle \boldsymbol{A}^{\rm ar}\cdot\boldsymbol{B}^{\rm ar}\rangle}{L_{\rm ar}\,\langle(\boldsymbol{B}^{\rm ar})^2\rangle}. \tag{22}$$

The total magnetic helicity $H_{\rm total}$ is conserved. Owing to a non-zero flux of magnetic helicity, part of the total magnetic helicity is transported to the chromosphere and corona from the active region. This implies that the total magnetic helicity $H_{\rm total} \equiv \langle \boldsymbol{A}^{\rm ar}\cdot\boldsymbol{B}^{\rm ar}\rangle\, V$ is the sum of the transported magnetic helicity, $H_{\rm transp}$, and the residual magnetic helicity (i.e. the observable magnetic helicity), $H_{\rm observ}$:

$$H_{\rm total} = H_{\rm transp} + H_{\rm observ}, \tag{23}$$

where V is the volume occupied by the active region. Here we assume that the transported magnetic helicity, $H_{\rm transp}$, is the sum of the magnetic helicity caused by the writhe of the active region, $C_w\,\langle \boldsymbol{A}^{\rm ar}\cdot\boldsymbol{B}^{\rm ar}\rangle\, V$ (with $C_w < 1$), and the magnetic helicity, $C_\Omega\,\langle(\boldsymbol{B}^{\rm ar})^2\rangle\,\gamma\,L_{\rm ar}\,V$, produced by the mechanical twist of the magnetic flux tube due to the Coriolis force:

$$H_{\rm transp} = \left(C_w\,\langle \boldsymbol{A}^{\rm ar}\cdot\boldsymbol{B}^{\rm ar}\rangle + C_\Omega\,\langle\left(\boldsymbol{B}^{\rm ar}\right)^2\rangle\,\gamma\,L_{\rm ar}\right) V, \tag{24}$$

where γ is the mean tilt discussed in Sections 2–4. The observed mean tilt is defined as

$$\gamma_{\rm observ} = \frac{H_{\rm observ}}{\langle(\boldsymbol{B}^{\rm ar})^2\rangle\,L_{\rm ar}\,V}. \tag{25}$$

The total magnetic helicity $H_{\rm total} \equiv \gamma_H L_{\rm ar}\,\langle(\boldsymbol{B}^{\rm ar})^2\rangle\,V$ is conserved. Substituting equations (24) into equation (23), and using equations (22) and (25), we obtain

$$\gamma_{\rm observ} = (1-C_w)\,\gamma_H - C_\Omega\,\gamma. \tag{26}$$

Because $\gamma_H \propto L_{\rm ar}^{-1}$ and $\gamma \propto L_{\rm ar}^2$, we obtain that $|\gamma_H| \ll |\gamma|$ for large-size active regions, where we take into account that $\delta_0 \propto L_B^2 \geq L_{\rm ar}^2$. This implies that $C_\Omega = -1$, because in this case $\gamma_{\rm observ} \approx \gamma$. On the other hand, for small-size active regions $|\gamma_H| \gg |\gamma|$. In the general case, both terms in equation (26) are important, so that the observable tilt is given by

$$\gamma_{\rm observ} = \gamma + (1-C_w)\,\frac{\langle \boldsymbol{A}^{\rm ar}\cdot\boldsymbol{B}^{\rm ar}\rangle}{L_{\rm ar}\,\langle(\boldsymbol{B}^{\rm ar})^2\rangle}, \tag{27}$$

where we use equation (20). It follows from this equation that there is a size of bipolar region for which the two contributions to the mean tilt are of the same order. This is in qualitative agreement with the study by Illarionov et al. (2015) and Tlatova & Tlatov (2019). Note that $\langle \boldsymbol{A}^{\rm ar}\cdot\boldsymbol{B}^{\rm ar}\rangle = -\overline{\boldsymbol{A}}\cdot\overline{\boldsymbol{B}}$ (Zhang et al. 2012), so that

$$\gamma_{\rm observ} = \gamma - (1-C_w)\,\frac{\overline{\boldsymbol{A}}\cdot\overline{\boldsymbol{B}}}{L_{\rm ar}\,\langle(\boldsymbol{B}^{\rm ar})^2\rangle}. \tag{28}$$

Using equations (13) and (28), we obtain

$$\begin{aligned}\gamma_{\rm observ} = &-\tilde{\delta}_0\Big[\sin\phi + \delta_3\sin 3\phi - \delta_5\sin 5\phi\\ &-\tilde{\delta}_M\left(\cos\phi + \tilde{\delta}_3\cos 3\phi - \tilde{\delta}_5\cos 5\phi\right)\Big]\\ &-(1-C_w)\,\frac{\overline{\boldsymbol{A}}\cdot\overline{\boldsymbol{B}}}{L_{\rm ar}\,\langle(\boldsymbol{B}^{\rm ar})^2\rangle}.\end{aligned} \tag{29}$$

In the northern hemisphere, $\overline{\boldsymbol{A}}\cdot\overline{\boldsymbol{B}}$ is negative, which implies that the sign of the last term describing the contribution caused by the magnetic helicity of the active region is opposite to that due to the contribution from the Coriolis force (the γ term). This implies that the mean tilts caused by the large-size and small-size active regions have opposite signs.

This explains the difference between Figs 1 and 4 in the vicinity of the equator. Indeed, in Fig. 4 the mean tilt determined by averaging over only large-size bipolar regions is not zero in the vicinity of the equator. In contrast, in Fig. 1 the mean tilt determined by averaging over all active regions tends to zero in the vicinity of the equator. The physical reason for this is as follows. Because the mean tilts caused by the large-size and small-size active regions have opposite signs, the mean tilt calculated by averaging over all active regions is small, because their contributions compensate each other. This implies that in the vicinity of the equator, the mean tilt is less than that calculated by averaging over only large-size bipolar regions. Recall that the effect of the Coriolis force on the mean tilt vanishes in the vicinity of the equator, so that the above effect of the compensation of the contributions to the mean tilt caused by the large-size and small-size active regions is more pronounced in the vicinity of the equator.

6 CONCLUSIONS

We have developed a theory of the mean tilt of sunspot bipolar regions. The formation of the mean tilt is caused by the effect of the Coriolis force on meso-scale motions of super-granular convection and large-scale meridional circulation. We have demonstrated that at low latitudes, the joint action of the Coriolis force and the magnetic tension results in an additional magnetic contribution to the mean tilt of the sunspot bipolar regions, which depends on the large-scale magnetic field. We have also found an additional contribution to the mean tilt of the sunspot bipolar regions caused by the effect of the latitudinal dependence of the solar differential rotation on the mean tilt. The latter phenomenon can explain the deviations from Joy's law for the mean tilt at higher latitudes. Our theoretical results and numerical simulations for the mean tilt are in an agreement with observational data of the mean tilt of sunspot bipolar regions.

ACKNOWLEDGEMENTS

The detailed comments on our manuscript provided by the anonymous referee are very much appreciated. Stimulating discussions with participants of the NORDITA programs on 'Solar Helicities in Theory and Observations: Implications for Space Weather and Dynamo Theory' (March 2019) and 'The Shifting Paradigm of Stellar Convection: From Mixing Length Concept to Realistic Turbulence Modelling' (March 2020) are acknowledged. The work of KK and NS was supported in part by a grant from the Russian Science Foundation (grant RNF 18-12-00131) at the Crimean Astrophysical Observatory. AT would like to acknowledge support from RFBR grant 18-02-00098 for the observational data analysis. NK, KK, IR acknowledge the hospitality of NORDITA.

REFERENCES

Babcock H. W., 1961, ApJ, 133, 572
Baker N., Temesvary S., 1966, Tables of Convective Stellar Envelope Models, NASA, New York
Belvedere G., Kuzanyan K. M., Sokoloff D., 2000, MNRAS, 315, 778

Berdyugina S. V., Moss D., Sokoloff D., Usoskin I. G., 2006, A&A, 445, 703
Bigazzi A., Ruzmaikin A., 2004, ApJ, 604, 944
Brandenburg A., Subramanian K., 2005, Phys. Rep., 417, 1
Brandenburg A., Kemel K., Kleeorin N., Mitra D., Rogachevskii I., 2011, ApJ, 740, L50
Brandenburg A., Kleeorin N., Rogachevskii I., 2013, ApJ, 776, L23
Brandenburg A., Gressel O., Jabbari S., Kleeorin N., Rogachevskii I., 2014, A&A, 562, A53
Brandenburg A., Rogachevskii I., Kleeorin N., 2016, New J. Phys., 18, 125011
Choudhuri A. R., Chatterjee P., Jiang J., 2007, Phys. Rev. Lett., 98, 131103
D'Silva S., Choudhuri A. R., 1993, A&A, 272, 621
Dasi-Espuig M., Solanki S. K., Krivova N. A., Cameron R., Peñuela T., 2010, A&A, 518, A7
Dikpati M., Gilman P. A., 2006, ApJ, 649, 498
Drobyshevski E. M., Yuferev V. S., 1974, J. Fluid Mech., 65, 33
Fisher G. H., Fan Y., Longcope D. W., Linton M. G., Pevtsov A. A., 2000, Solar Phys., 192, 119
Frisch U., Pouquet A., Leorat I., Mazure A., 1975, J. Fluid Mech., 68, 769
Gibson E. G., 1973, The Quiet Sun, NASA, Washington
Gilman P. A., 1970, ApJ, 162, 1019
Glatzmaier G., 1985, ApJ, 291, 330
Hale G. E., Ellerman F., Nicholson S. B., Joy A. H., 1919, ApJ, 49, 153
Holder Z. A., Canfield R. C., McMullen R. A., Nandy D., Howard R. F., Pevtsov A. A., 2004, ApJ, 611, 1149
Howard R. F., 1991, Solar Phys., 136, 251
Illarionov E., Tlatov A., Sokoloff D., 2015, Solar Phys., 290, 351
Kleeorin N., Rogachevskii I., 1994, Phys. Rev. E, 50, 2716
Kleeorin N., Rogachevskii I., 1999, Phys. Rev. E, 59, 6724
Kleeorin N., Ruzmaikin A., 1982, Magnetohydrodynamics, 18, 116, translated from Magnitnaya Gidrodinamika, 2, 17
Kleeorin N., Ruzmaikin A., 1991, Solar Phys., 131, 211
Kleeorin N., Rogachevskii I., Ruzmaikin A. A., 1989, Sov. Astron. Lett., 15, 274
Kleeorin N., Rogachevskii I., Ruzmaikin A. A., 1990, Sov. Phys. JETP, 70, 878
Kleeorin N., Mond M., Rogachevskii I., 1993, Phys. Fluids B, 5, 4128
Kleeorin N., Rogachevskii I., Ruzmaikin A., 1995, A&A, 297, 159
Kleeorin N., Mond M., Rogachevskii I., 1996, A&A, 307, 293
Kleeorin N., Moss D., Rogachevskii I., Sokoloff D., 2000, A&A, 361, L5
Kleeorin N., Moss D., Rogachevskii I., Sokoloff D., 2002, A&A, 387, 453
Kleeorin N., Kuzanyan K., Moss D., Rogachevskii I., Sokoloff D., Zhang H., 2003a, A&A, 409, 1097
Kleeorin N., Moss D., Rogachevskii I., Sokoloff D., 2003b, A&A, 400, 9
Kleeorin Y., Safiullin N., Kleeorin N., Porshnev S., Rogachevskii I., Sokoloff D., 2016, MNRAS, 460, 3960
Kosovichev A. G., Stenflo J. O., 2008, ApJ, 688, L115
Krause F., Rädler K.-H., 1980, Mean-Field Magnetohydrodynamics and Dynamo Theory. Pergamon, Oxford
Krivodubskiy V. N., 1998, Astron. Rep., 42, 122
Kuzanyan K. M., Lamburt V. G., Zhang H., Bao S., 2003, Chinese J. Astron. Astrophys., 3, 257
LaBonte B. I., Howard R., 1982, Solar Phys., 75, 161
Leighton R. B., 1969, ApJ, 156, 1
Livshits I. M., Obridko V. N., 2006, Astron. Rep., 50, 926
Longcope D., Linton M., Pevtsov A., Fisher G., Klapper I., 1999, in Brown M. R., Canfield R. C., Pevtsov A. A., eds, Magnetic Helicity in Space and Laboratory Plasmas, Geophysical Monograph Ser. 111, American Geophysical Union, Washington, p. 93
McClintock B. H., Norton A. A., 2013, Solar Phys., 287, 215
McClintock B. H., Norton A. A., 2016, ApJ, 818, 7
McClintock B. H., Norton A. A., Li J., 2014, ApJ, 797, 130
Moffatt H. K., 1978, Magnetic Field Generation in Electrically Conducting Fluids. Cambridge Univ. Press, New York
Norton A. A., Gilman P. A., 2005, ApJ, 630, 1194
Ossendrijver M., 2003, A&A*R*, 11, 287
Parker E., 1955, ApJ, 121, 491
Parker E., 1966, ApJ, 145, 811
Parker E., 1979, Cosmical Magnetic Fields. Clarendon, Oxford
Pevtsov A. A., Berger M. A., Nindos A., Norton A. A., van Driel-Gesztelyi L., 2014, Space Sci. Rev., 186, 285
Pipin V. V., Kosovichev A. G., 2015, ApJ, 813, 134
Pouquet A., Frisch U., Leorat J., 1976, J. Fluid Mech., 77, 321
Priest E. R., 1982, Solar Magnetohydrodynamics. Reidel, Dordrecht
Rogachevskii I., Kleeorin N., 2000, Phys. Rev. E, 61, 5202
Rogachevskii I., Kleeorin N., 2001, Phys. Rev. E., 64, 056307
Rogachevskii I., Kleeorin N., 2004, Phys. Rev. E, 70, 046310
Rogachevskii I., Kleeorin N., 2007, Phys. Rev. E, 76, 056307
Rüdiger G., Hollerbach R., 2004, The Magnetic Universe. Wiley-VCH, Weinheim
Safiullin N., Kleeorin N., Porshnev S., Rogachevskii I., Ruzmaikin A., 2018, J. Plasma Phys., 84, 735840306
Schüssler M., Caligari P., Ferriz-Mas A., Moreno-Insertis F., 1994, A&A, 281, L69
Sivaraman K. R., Gupta S. S., Howard R. F., 1999, Solar Phys., 189, 69
Spiegel E. A., Weiss N. O., 1980, Nature, 287, 616
Spruit H. C., 1974, Solar Phys., 34, 277
Spruit H. C., 1981, A&A, 98, 155
Spruit H. C., van Ballegooijen A. A., 1982, A&A, 106, 58
Stix M., 1989, The Sun: An Introduction, Springer, Heidelberg
Tlatov A. G., 2015, Adv. Space Res., 55, 851
Tlatova K. A., Tlatov A. G., 2019, in Bipoles that violate the laws of Joy and Hale in the 15–24th activity cycles. In Proc. 23 Russian Annual Meeting-2019 'Solar and Solar-Terrestrial Physics'. GAO RAN, Sant-Petersburg, p. 395
Tlatov A. G., Illarionov E., Sokoloff D., Pipin V., 2013, MNRAS, 432, 2975
Tlatova K. A., Vasileva V. V., Pevtsov A. A., 2015, Geomagn. Aeron., 55, 896
Tlatova K., Tlatov A., Pevtsov A., Mursula K., Vasileva V., Heikkinen E. et al., 2018, Solar Phys., 293, 118
Tobias S. M., Hughes D. W., 2004, ApJ, 603, 785
Tobias S. M., Brummell N. H., Clune T. L., Toomre J., 2001, ApJ, 549, 1183
Warnecke J., Losada I. R., Brandenburg A., Kleeorin N., Rogachevskii I., 2013, ApJ, 777, L37
Warnecke J., Losada I. R., Brandenburg A., Kleeorin N., Rogachevskii I., 2016, A&A, 589, A125
Weiss N. O., 1966, Proc. R. Soc. Lond., A293, 310
Yoshimura H., 1981, ApJ, 247, 1102
Zeldovich Ya. B., Ruzmaikin A. A., Sokoloff D. D., 1983, Magnetic Fields in Astrophysics, Gordon and Breach, New YorK
Zhang H., Sokoloff D., Rogachevskii I., Moss D., Lamburt V., Kuzanyan K., Kleeorin N., 2006, MNRAS, 365, 276
Zhang H., Moss D., Kleeorin N., Kuzanyan K., Rogachevskii I., Sokoloff D., Gao Y., Xu H., 2012, ApJ, 751, 47

APPENDIX A: DERIVATION OF EQUATIONS (5), (7) AND (13)

To derive equation (5), we rewrite equations (2) and (3) for small perturbations $\tilde{\boldsymbol{b}}$ and $\tilde{s}$ as

$$\tilde{\boldsymbol{b}} = (\boldsymbol{B}^{\rm eq}\cdot\nabla)\boldsymbol{\xi} - (\boldsymbol{\xi}\cdot\nabla)\boldsymbol{B}^{\rm eq} - \Lambda_\rho\,\boldsymbol{B}^{\rm eq}\,(\hat{\boldsymbol{r}}\cdot\boldsymbol{\xi}), \tag{A1}$$

$$\tilde{s} = -(\boldsymbol{\xi}\cdot\nabla)S^{\rm eq} - \frac{\Omega_b^2}{g}\,\boldsymbol{\xi}\cdot\hat{\boldsymbol{r}}. \tag{A2}$$

Substituting equations (A1) and (A2) into equation (1) rewritten for small perturbations $\boldsymbol{\xi}$, we obtain equation (5). In the derivation of equation (5), we use assumptions (6) outlined in Section 2.

To derive equation (7) for the mean tilt of sunspot bipolar regions, we exclude the pressure term from equation (5) by applying curl to this equation and multiplying the obtained equation by the unit vector $\boldsymbol{e}_B = \boldsymbol{B}^{\rm eq}/B^{\rm eq}$. This yields

$$\frac{\partial^2 \tilde{\gamma}}{\partial t^2} = 2\left[\nabla \times \left(\left(\boldsymbol{U}^{\rm eq} + \frac{\partial \boldsymbol{\xi}}{\partial t} + \boldsymbol{v}^{(\rm c)}\right) \times \boldsymbol{\Omega}\right)\right] \cdot \boldsymbol{e}_B + (\boldsymbol{U}_{\rm A} \cdot \nabla)^2\, \delta_B, \tag{A3}$$

where $\tilde{\gamma} = \boldsymbol{\delta}^{\rm tw} \cdot \boldsymbol{e}_B$ is the tilt, $\boldsymbol{\delta}^{\rm tw} = \nabla \times \boldsymbol{\xi}$. Here we take into account that at the boundary between the convective zone and the photosphere, the magnetic field inside the sunspots is preferably directed in the radial direction. Because the second and the last terms in equation (5) are directed in the radial direction, they do not contribute to the $\hat{\boldsymbol{r}}$ component of the curl; that is, they do not contribute to $\tilde{\gamma}$.

We seek the solution of equation (A3) in the form of standing Alfvén waves as

$$\tilde{\gamma} = \sum_{m=0}^{\infty} A_m \cos\left[\frac{(2m+1)\pi\zeta}{L_B}\right] \cos\left[\frac{2\pi t}{T_m} + \varphi\right], \tag{A4}$$

where $T_m = 2\tau_{\rm A}/(2m+1)$ is the period of non-dissipating oscillations, $\tau_{\rm A} = L_B/U_{\rm A}$ is the Alfvén time, and ζ is the coordinate along the magnetic field line of length L_B connecting sunspots of opposite magnetic polarities. Now we take into account that $T_m\,\Omega \ll 1$, which implies that $|\partial\boldsymbol{\xi}/\partial t| \ll |\boldsymbol{v}^{(\rm c)}|, |\boldsymbol{U}^{\rm eq}|$. We also assume that the source of the tilt $I_\gamma = 2[\nabla \times [(\boldsymbol{U}^{\rm eq} + \boldsymbol{v}^{(\rm c)}) \times \boldsymbol{\Omega}]] \cdot \boldsymbol{e}_B$ in equation (A3) is localized near the boundary between the solar convective zone and the photosphere. This source can be modelled as the combination of two Dirac delta functions:

$$I_\gamma(\zeta) = 2\Big[\nabla \times [(\boldsymbol{U}^{\rm eq} + \boldsymbol{v}^{(\rm c)}) \times \boldsymbol{\Omega}]\Big] \cdot \boldsymbol{e}_B \times \Big[\delta(\zeta/L_B) - \delta(\zeta/L_B - 1)\Big], \tag{A5}$$

where $\delta(x)$ is the Dirac delta function.

We substitute equation (A4) into equation (A3), and after the Fourier transformation of the source term (A5), we obtain the equation for the amplitude $A_m(t)$ as

$$\frac{\partial^2 A_m}{\partial t^2} = \frac{2I_\gamma}{\pi} - \left[U_{\rm A}\,\frac{(2m+1)\pi}{L_B}\right]^2 A_m. \tag{A6}$$

This equation with initial condition $A_m(t=0) = 0$ has the following solution:

$$A_m(t) = \frac{2I_\gamma\,\tau_{\rm A}^2}{\pi^3(2m+1)^2}\left\{1 - \cos\left[\frac{(2m+1)\,\pi\,t}{\tau_{\rm A}}\right]\right\}. \tag{A7}$$

Substituting equation (A7) into equation (A4), we obtain the expression for $\tilde{\gamma}$ as

$$\tilde{\gamma} = \frac{2I_\gamma\,\tau_{\rm A}^2}{\pi^3} \sum_{m=0}^{\infty} \frac{1}{(2m+1)^2} \cos\left[\frac{(2m+1)\pi\zeta}{L_B}\right] \times \left\{1 - \cos\left[\frac{(2m+1)\,\pi\,t}{\tau_{\rm A}}\right]\right\}. \tag{A8}$$

Averaging equation (A8) over a time that is longer than the maximum Alfvén time $\tau_{\rm A}$, we obtain equation (7) for the mean tilt $\gamma = \langle\tilde{\gamma}\rangle_{\rm time}$ of sunspot bipolar regions at the surface of the Sun.

For the derivation of equation (13), we used the identities given below:

$$\sin^3\phi = \frac{1}{4}\,[3\sin\phi - \sin 3\phi]\,, \tag{A9}$$

$$\sin^5\phi = \frac{1}{16}\,[10\sin\phi - 5\sin 3\phi + \sin 5\phi]\,, \tag{A10}$$

$$\sin^2\phi\,\cos\phi = \frac{1}{4}\,[\cos\phi - \cos 3\phi]\,, \tag{A11}$$

$$\sin^4\phi\,\cos\phi = \frac{1}{16}\,[2\cos\phi - 3\cos 3\phi + \cos 5\phi]\,. \tag{A12}$$

APPENDIX B: EQUATION FOR THE RADIAL MEAN VELOCITY

The momentum equation (1) with additional force caused by the eddy viscosity in a steady state in spherical coordinates reads

$$\frac{\partial}{\partial r}\overline{P}_{\rm tot} = \frac{2}{r^2}\frac{\partial}{\partial r}\left(r^2\frac{\rho_0\,\overline{U}_r\,\nu_T}{H_\rho}\right) - \frac{\overline{B}_\varphi^2}{4\pi r} + 2\rho_0\,\overline{U}_\varphi\,\Omega\,\sin\theta + \frac{1}{r\,\sin\theta}\frac{\partial}{\partial\theta}\left(\sin\theta\,\frac{\rho_0\,\overline{U}_\theta\,\nu_T}{H_\rho}\right), \tag{B1}$$

$$\frac{\partial}{\partial\theta}\overline{P}_{\rm tot} = \frac{1}{r^2}\frac{\partial}{\partial r}\left(r^3\frac{\rho_0\,\overline{U}_\theta\,\nu_T}{H_\rho}\right) - \frac{\overline{B}_\varphi^2}{4\pi}\cot\theta + 2\rho_0\,\overline{U}_\varphi\,\Omega\,r\,\cos\theta, \tag{B2}$$

where, $\overline{P}_{\rm tot} = \overline{P} + \overline{\boldsymbol{B}}^2/8\pi + \overline{\boldsymbol{U}}^2/2$ is the total pressure, H_ρ is the density height-scale, and ν_T is the eddy viscosity.

We exclude the total pressure term, use the continuity equation $\nabla \cdot (\rho_0\,\overline{\boldsymbol{U}}) = 0$, and introduce the stream function Ψ:

$$\rho_0\,\overline{U}_r = \frac{1}{r^2\sin\theta}\frac{\partial\Psi}{\partial\theta}, \quad \rho_0\,\overline{U}_\theta = -\frac{1}{r\sin\theta}\frac{\partial\Psi}{\partial r}. \tag{B3}$$

After neglecting a weak dependence of ν_T/H_ρ on radius r, equations (B1)–(B2) are reduced to

$$\frac{\partial^2 Y}{\partial X^2} + \frac{1}{9X^2}\frac{\partial}{\partial\theta}\left(\frac{1}{\sin\theta}\frac{\partial}{\partial\theta}(Y\sin\theta)\right) = f(X,\theta), \tag{B4}$$

where $X = r^3$, $\quad Y = X\,\rho_0\,\overline{U}_\theta\,\nu_T/H_\rho$, and

$$f(X,\theta) = \frac{1}{36\pi}\left(\frac{1}{X}\frac{\partial}{\partial\theta} - \frac{3}{\tan\theta}\frac{\partial}{\partial X}\right)\overline{B}_\varphi^2. \tag{B5}$$

Here we take into account that the contribution of the Coriolis force to the function $f(X,\theta)$ under the condition of slow rotation is small (Kleeorin & Ruzmaikin 1991; Kleeorin et al. 1996). The solution of equation (B4) with the boundary condition

$$\left[(1-\kappa)\,\frac{\partial(\rho_0\,\overline{U}_r)}{\partial r} + \frac{2\rho_0\,\overline{U}_r}{r}\right]_{r=\rm R_\odot} = 0 \tag{B6}$$

is given by

$$\overline{U}_r = \frac{\ell_0^2}{4\pi\,\kappa\,\nu_T\,\rho_{\rm top}\,\rm R_\odot}\,\frac{1}{\sin\theta}\,\frac{\partial}{\partial\theta}\Big[\sin\theta\,F(\theta)\Big], \tag{B7}$$

where the parameter $\kappa \approx 0.3$–0.4 characterizes the fraction of the large-scale radial momentum of the plasma that is lost as it crosses the boundary between the convective zone and photosphere, and

$$F(\theta) \approx \int_{\rm R_\odot - L}^{\rm R_\odot}\left(1 + \frac{\rm R_\odot - r}{L - \ell_0}\right)\left(\frac{\partial\overline{\boldsymbol{B}}^2}{u\partial\theta}\right)\frac{{\rm d}r}{r} \approx C_u\left(\frac{\partial\overline{\boldsymbol{B}}^2}{\partial\theta}\right)_{\rm bot}, \tag{B8}$$

where the constant C_u varies from 0.7 to 1, depending on the radial profile of the mean magnetic field. Therefore, equations (B7)–(B8) yield equation (9).

APPENDIX C: THE EVOLUTION OF THE WOLF NUMBER

In the framework of the non-linear mean-field dynamo model by Kleeorin et al. (2016) and Safiullin et al. (2018), the phenomenological budget equation for the surface density of the Wolf number is given by

$$\frac{\partial \tilde{W}}{\partial t} = I_{\rm w}(t,\theta) - \frac{\tilde{W}}{\tau_s(\overline{B})}, \tag{C1}$$

where the rate of increase of the surface density of the Wolf number caused by the formation of sunspots is

$$I_{\rm w}(t,\theta) = \frac{|\gamma_{\rm inst}||\overline{B}-\overline{B}_{\rm cr}|}{\Phi_s}\Theta(\overline{B}-\overline{B}_{\rm cr}), \tag{C2}$$

and the rate of decay of sunspots is $\tilde{W}/\tau_s(\overline{B})$ with the decay time, $\tau_s(\overline{B})$, of sunspots, and $\Theta(x)$ is the Θ function, defined as $\Theta(x)=1$ for $x>0$, and as $\Theta(x)=0$ for $x\le 0$. Here, $\overline{B}_{\rm cr}$ is the threshold for the sunspot formation, and $\gamma_{\rm inst}$ is the inverse time of the formation of sunspots.

As an example for the estimation of the parameters $\overline{B}_{\rm cr}$ and $\gamma_{\rm inst}$, we use in the present study the negative effective magnetic pressure instability (Kleeorin et al. 1989, 1990, 1993, 1996; Kleeorin & Rogachevskii 1994; Rogachevskii & Kleeorin 2007) resulting in the formation of magnetic spots (Brandenburg et al. 2011; Brandenburg et al. 2013, 2014) and bipolar active regions (Warnecke et al. 2013, 2016). The growth rate $\gamma_{\rm inst}$ of the negative effective magnetic pressure instability is given by

$$\gamma_{\rm inst} = \left(\frac{2\overline{U}_{\rm A}^2 k_x^2}{H_\rho^2 k^2}\left|\frac{{\rm d}P_{\rm eff}}{{\rm d}\beta^2}\right| - \frac{4(\boldsymbol{\Omega}\cdot\boldsymbol{k})^2}{\boldsymbol{k}^2}\right)^{1/2} - \eta_T\left(k^2+\frac{1}{(2H_\rho)^2}\right) \tag{C3}$$

(Rogachevskii & Kleeorin 2007; Brandenburg et al. 2016), where $\overline{U}_{\rm A}=\overline{\rm B}/(4\pi\rho_0)^{1/2}$ is the Alfvén speed based on the mean magnetic field, $\boldsymbol{k}$ is the wavenumber, $P_{\rm eff}=\frac{1}{2}\left[1-q_{\rm p}(\beta)\right]\beta^2$ is the effective magnetic pressure, the non-linear function $q_{\rm p}(\beta)$ is the turbulence contribution to the mean magnetic pressure, and $\beta=\overline{B}/\overline{B}_{\rm eqp}$. We assume here that the characteristic time of the Wolf number variations is of the order of the characteristic time for the excitation of the instability, $\gamma_{\rm inst}^{-1}$. When the instability is not excited ($\gamma_{\rm inst}<0$), the production rate of sunspots $I_{\rm w}(t,\theta)\to 0$, which means that the function $I_{\rm w}(t,\theta)\propto|\gamma_{\rm inst}|\,\Theta(\overline{B}-\overline{B}_{\rm cr})$. The production term of sunspots is also proportional to the maximum number of sunspots per unit area, which is estimated as $\sim|\overline{B}-\overline{B}_{\rm cr}|/\Phi_s$, where $|\overline{B}-\overline{B}_{\rm cr}|$ is the magnetic flux per unit area that contributes to the sunspot formation, and Φ_s is the magnetic flux inside a magnetic spot. This instability is excited when the mean magnetic field is stronger than a critical value, $\overline{B}>\overline{B}_{\rm cr}$:

$$\frac{\overline{B}_{\rm cr}}{\overline{B}_{\rm eq}} = \frac{\ell_0}{50H_\rho}\left[1+\left(\frac{10\,{\rm Co}\,H_\rho^2}{\ell_0^2}\right)^2\right]^{1/2}. \tag{C4}$$

This instability is excited in the upper part of the convective zone, where the Coriolis number ${\rm Co}=2\Omega\tau$ is small. The decay time $\tau_s(\overline{B})$ varies from several weeks to a couple of months, while the solar cycle period is about 11 yr. This means that we can use the steady-state solution of equation (C1), $\tilde{W}=\tau_s(\overline{B})\,I_{\rm w}(t,\theta)$. The Wolf number is defined as a surface integral as $W=R_\odot^2\int\tilde{W}(t,\theta)\sin\theta\,{\rm d}\theta\,{\rm d}\varphi=2\pi R_\odot^2\int\tau_s(\overline{B})\,I(t,\theta)\sin\theta\,{\rm d}\theta$. The function $\tau_s(\overline{B})$ is given by $\tau_s(\overline{B})=\tau_*\exp\left(C_{\rm s}\,\partial\overline{B}/\partial t\right)$, where $C_{\rm s}=1.8\times10^{-3}$ and $\gamma_{\rm inst}\,\tau_*\sim 10$.

There are also other mechanisms for the formation of inhomogeneous magnetic structures, for example the magnetic buoyancy instability (or interchange instability) of a stratified continuous magnetic field (Parker 1966; Gilman 1970; Priest 1982), magnetic flux expulsion (Weiss 1966), topological magnetic pumping (Drobyshevski & Yuferev 1974), etc. Magnetic buoyancy is applied in the literature in various situations. One relates to the magnetic buoyancy instability of a stratified continuous magnetic field (Parker 1966; Gilman 1970; Priest 1982), and the magnetic flux tube concept is not used there. Another describes the buoyancy of discrete magnetic flux tubes discussed in various contexts in solar physics and astrophysics (Parker 1955; Spruit 1981; Spruit & van Ballegooijen 1982; Schüssler et al. 1994; Dikpati & Gilman P. 2006; Choudhuri, Chatterjee & Jiang 2007). This is related to the problem of the storage of magnetic fields in the overshoot layer near the bottom of the solar convective zone (Spiegel & Weiss 1994; Tobias et al. 2001; Tobias & Hughes 2004).

The growth rate of the magnetic buoyancy instability reads

$$\gamma_{\rm inst} = \frac{\overline{U}_{\rm A}}{H_\rho}\left[Q_{\rm p}\left(\frac{H_\rho}{\tilde{L}_B}-1\right)\right]^{1/2} - \eta_T k^2, \tag{C5}$$

where $\tilde{L}_B$ is the characteristic scale of the initial mean magnetic field variations, and $Q_{\rm p}=1-q_{\rm p}(\beta)$. Without turbulence, $Q_{\rm p}=1$ and the magnetic buoyancy instability of a stratified continuous magnetic field is excited when the scale of variations of the initial magnetic field is less than the density stratification length. The source of free energy for the magnetic buoyancy instability is the energy of the gravitational field. Generally, the critical magnetic field $\overline{B}_{\rm cr}$ and the growth rate $\gamma_{\rm inst}$ for the magnetic buoyancy instability can be used for the estimation of the rate of production of the Wolf number density given by equation (C2).

However, in the presence of strong turbulence, $Q_{\rm p}$ can be negative, and the negative effective magnetic pressure instability can be excited. The source of free energy for the negative effective magnetic pressure instability is the energy of turbulence or turbulent convection.

This paper has been typeset from a TEX/LATEX file prepared by the author.